ORIGINAL ARTICLE

Obtaining a fused PLA-calcium phosphate-tobramycin-based filament for 3D printing with potential antimicrobial application

Alex A. Lopera[1,2] · Vinicius D. N. Bezzon[3] · Victoria Ospina[4] · Jorge L. Higuita-Castro[4] · Francisco J. Ramirez[5] · Humberto G. Ferraz[6] · Marcos T. A. Orlando[3] · Carlos G. Paucar[1] · Sara M. Robledo[4] · Claudia P. Garcia[1]

Abstract

Many efforts in the tissue engineering field have been devoted to producing biomedical devices with several physico-chemical properties that could promote an increase in the quality of therapeutic treatments. Thus, 3D printing is an efficient method which facilitates manufacturing high quality products to be used as medical devices. However, high-performance materials are required for obtaining products that are able to be 3D printed to attend the biomedical concerns. In this work, fused PLA-calcium phosphate-tobramycin-based filaments with antimicrobial properties were produced. X-ray powder diffraction, Fourier transform infrared spectroscopy and thermal analysis were performed to characterize the pure compounds as well as the composite filaments, revealing that the drug is preserved into the filaments by the implemented methodology, even after the hot extrusion procedure. The filaments and the printed pieces presented great antimicrobial effect and a controlled-release profile was also observed by the drug-release assays for the filaments produced, thereby indicating this material as a promising candidate to be used for implantable medical devices in the future.

✉ Alex A. Lopera
aalopera@unal.edu.co

1   Grupo de Cerámicos y Vítreos, Escuela de Física, Universidad Nacional de Colombia, Calle 59A.63-20, 050034 Medellín, Colombia

2   Grupo de Nanoestructuras y Física Aplicada (NANOUPAR), Dirección Académica, Universidad Nacional de Colombia, Sede de La Paz, Km 9 vía Valledupar La Paz, 200001 La Paz, Colombia

3   Grupo de Física Aplicada, Departamento de Física, Centro de Ciências Exatas, Universidade Federal do Espírito Santo, Av. Fernando Ferrari, 514-Goiabeiras, Vitória, ES 29075-910, Brazil

4   PECET-Instituto de Investigaciones Médicas, Facultad de Medicina, Universidad de Antioquia, Calle 70 No. 52-21, 050010 Medellín, Colombia

5   Faculty of Engineering, Mechanical Department, Institución Universitaria Pascual Bravo, Calle 73 No. 73A–226, 050034 Medellín, Colombia

6   Laboratório de Desenvolvimento e Inovação Farmacotécnica (DEINFAR), Departamento de Farmácia, Faculdade de Ciências Farmacêuticas, Universidade de São Paulo, São Paulo, SP CEP 05508-080, Brazil

Graphical abstract
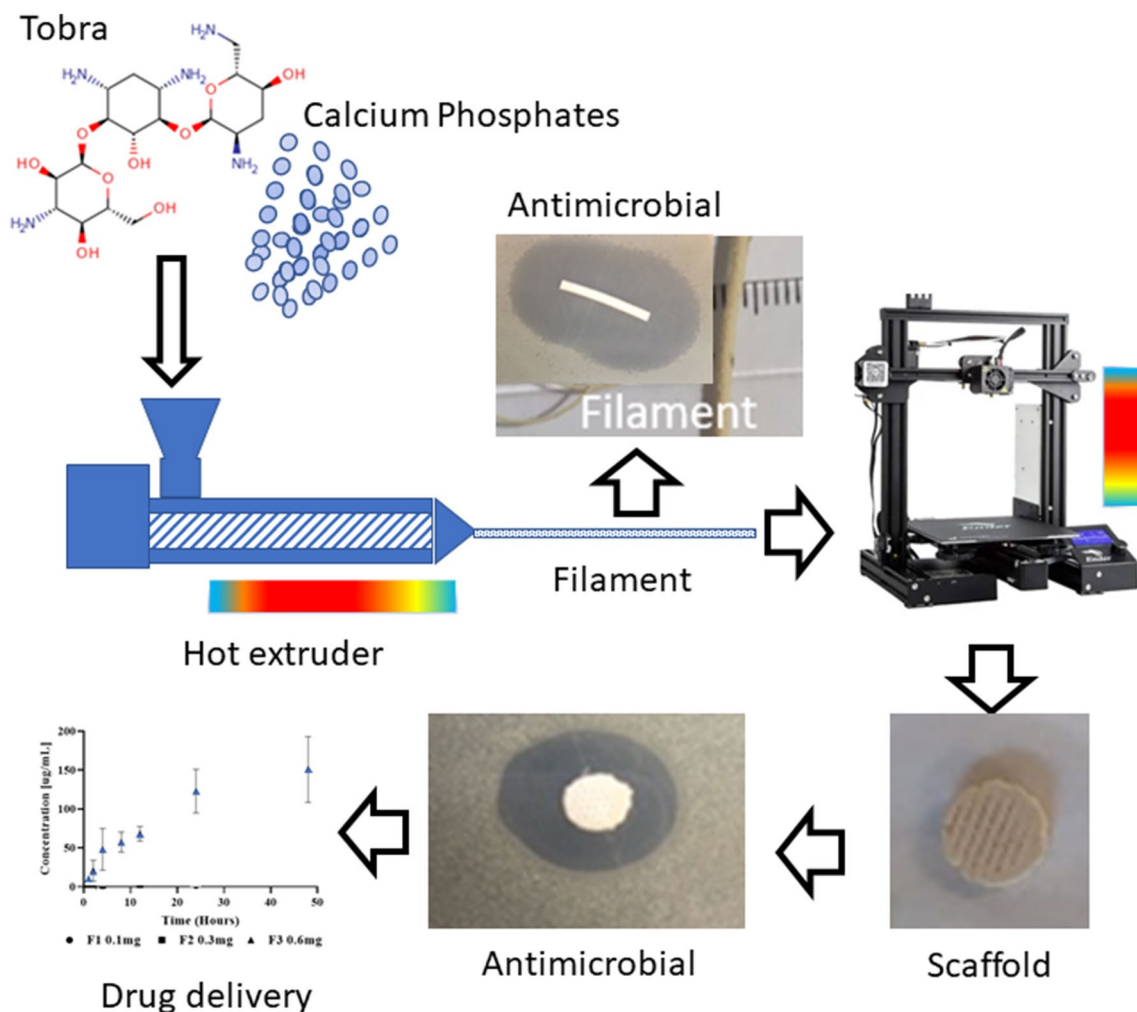
Keywords 3D printing · Filaments · Calcium phosphates · Tobramycin · Scaffolds · Antimicrobial

1 Introduction

3D printing technology has received significant attention in bone tissue engineering in recent years due to its versatility and precise control to produce medical devices such as scaffolds with customized shape and functionality [1]. This technology can be classified as additive manufacturing (AM), which is used to create pieces layer by layer from the 3D Computer-Aided design (CAD) model [2]. Fused deposition modeling (FDM) is one of the simplest and most cost-effective techniques employed in 3D printing of thermoplastic polymers with potential application in bone tissue engineering [3].

Many different works have focused on obtaining filaments with the appropriate properties to be used in scaffold fabrication and achieving suitable performance regarding therapeutic treatments concerns such as biocompatibility, biodegradation, and good mechanical properties [3–8]. However, optimizing FDM filaments to produce implantable medical devices by including other properties which provide antimicrobial activity as well as mechanical performance without compromising their biocompatibility is crucial for biomedical applications. Considering the mechanical performance, the main reason for implantable medical device failures are the infections associated with different kinds of pathogens such as *Staphylococcus aureus*, among others [9]. Bacterial infections can increase the possibility of developing osteomyelitis or other clinical complications associated with bacterial colonization with significant morbidity and sometimes death [3]. Previous reports estimate that around 2 to 5% of orthopedic implants are damaged by infection [10], and this can increase up to 30% in the case of open fractures

[11]. These complications can be treated by debriding infected tissue combined with the systemic antibiotic treatment over a long time, even in the case of implant removal to replace it with a new one. However, surgical intervention is unavoidable in both cases. All of these abovementioned problems lead to a decrease in the patient's quality of life. Furthermore, access to surgical interventions or implantable medical devices at the appropriate time are a public health problem in developing countries.

A way to overcome possible infections by pathogens in medical procedures which use implantable devices produced by FDM could be to load the filaments with antibiotics or antimicrobial nanoparticles which enable producing functionalized 3D-scaffolds with appropriate characteristics to be used as antimicrobial implantable medical devices. In this sense, polycraprolactone (PCL) has been explored as the potential drug-loading matrix in systems that incorporate antibiotics for manufacturing FDM filaments due to its low melting point which allows a wide use of drugs without losing their therapeutic activity. Scaffaro et al. incorporated chlorhexidine in polycaprolactone-based filaments and obtained a good antimicrobial response [12]. In addition, Viidik et al. used the active pharmaceutical ingredients such as indomethacin, ibuprofen, and anhydrous theophylline to produce 3D-printed tablets, demonstrating the polymer is suitable to be used in a polymeric carrier system [4].

Another polymer of great interest in bone tissue engineering is polylactic acid (PLA) which is one of the most common polyesters, and is approved by US food and drug administration (FDA) agency for human body applications. Several studies have shown the potential use of PLA in scaffold fabrication by 3D printing in providing antimicrobial response by means of functionalization including drugs like minocycline after its printing [13]. However, few studies have shown the incorporation of antibiotics directly into the PLA filament which enables obtaining antimicrobial functionalized scaffolds in one step by 3D printing. Water et al. obtained a nitrofurantoin-based filament, with this drug being used to avoid the formation of bacterial film [14]. This system was achieved by the hot-melting extrusion method, showing promising results in terms of drug release.

One of the possible antibiotics that has been extensively used for several applications is Tobramicyn (Tobra), with the molecular formula $C_{18}H_{37}N_5O_9$, which is obtained as a crystalline, white, and hygroscopic powder, freely soluble in water. It is an aminoglycoside antibiotic with a broad antibacterial spectrum used for several purposes in pharmaceutical applications such as ophthalmic solutions, suspensions, and intravenous, and oral administration [15]. Some systems using Tobra as the main antimicrobial agent have been proposed and studied to increase its oral absorption [16] or to prolongate the drug delivery in ophthalmic treatment [17]. Tobra also has the advantage of having a high melting point,

which allows this drug to be used in hot-melting extrudable systems, such as the FDM filaments. Other investigations of the potential application of the Tobra have been related to its use as the active pharmaceutical ingredient in local delivery systems for the treatment of infectious diseases such as osteomyelitis [18, 19]. This disease can affect any bone in the body and current therapies have shown some disadvantages, which includes the penetration of the antibiotic into the affected bone is not effective, and that the drug can affects the intended site as well as unaffected tissues that can raises the risks of cytotoxicity, nephrotoxicity and the potential for an increase in antibiotic resistance. For this reason the importance of finding alternative therapies such as local drug delivery systems could help overcome these disadvantages [20, 21]. From the crystallographic and characterization point-of-view, although Tobra has been broadly used and studied, no works have reported its crystal structure, which means that no crystal structures for this drug are currently available in the Cambridge Structural Database®, which provides access to crystal structures for organic compounds [22]. In addition, biphasic calcium phosphates (BCPs) are a potential bone substitute, because of their biocompatibility (they can form chemical bonds with bone) and osteoconductivity (they can support bone growth). BCPs are the mixture of hydroxyapatite (HAP) and β-tricalcium phosphate (TCP). These materials combine the resorbability of TCP, which is more soluble and its degradation products such as Ca^{2+} and PO_4^{3-} promote bioactivity, and at the same time maintain the osteoconductive potential of HAP presenting better results than when the HAP and TCP phases are used separately [23, 24]. BCPs have been used in scaffold fabrication in previous studies, where it is expected to obtain the degradation of the ceramic and the formation of new bone tissue through processes that occur simultaneously, thus ensuring optimal healing of the bone defect [25]. In a recent paper [26], we manufactured PLA/biphasic calcium phosphate-based filaments to be used in FDM using low-cost commercial printers. The filaments obtained presented adequate printability, the biological tests showed that ceramic-polymer filaments are potentially nontoxic and did not affect the proliferation of cells.

In the view of the above considerations, the main objective of this work was to obtain PLA-Calcium-Phosphate-Tobramicyn-based fused filaments which combine the excellent performance of BCPs in terms of osteoinductivity and bioactivity [27–34] with the potential antimicrobial response of the drug. It is worth noting that Tobra was chosen to be incorporated in the filaments due to its broad antimicrobial action, potential use in the treatment of infectious diseases that can affect the bone, and the relative high melting temperature, which allows it to be extruded without degradation. This one-step manufactured filament is a promising product because it decreases the acquisition cost and provides

interesting and desirable properties in implantable medical devices obtained by 3D printing that have potential use in systems for local drug delivery [35].

2 Materials and methods

2.1 Preparation of PLA/BCPS/Tobramycin composite and extrusion of composite filaments

First, 30 g of PLA/BCPs were prepared by a previously reported method [26]. BCP powders were made by the solution combustion route using calcium nitrate tetrahydrate $(Ca(NO_3)2.4(H_2O)$-Merck-Ca), diammonium hydrogen phosphate $((NH_4)2HPO_4$-Scharlau-P) as oxidant agent (O) and the glycine was employed as reducing agent (fuel- F). Next, the O and F were mixed in distilled water maintaining the stoichiometric ratio between O/F = 1 [36] to obtain the complete theoretical reaction with a ratio of Ca/P = 1.5. The mixture was heated to 80 °C with continuous stirring until gel formation, and the temperature was subsequently increased to 150 °C until combustion. The obtained powder was then thermally treated at a temperature of 800 °C for 2 h. To obtain the filament it was used a free-organic-solvent process similar to that reported by Corciene et al. [37] and Nevado et al. [26] with some modifications. Previously grounded commercial PLA Huaian Ruanke Trade Co with a molecular weight of 60,000–80,000 g/mol and specific gravity of 1.24 g/cc was used in this work. BCP powders were mixed with PLA in a ratio of 30% wt of BCP by means of a Retsch PM ball mill at 100 to 250 rpm for 15 min. In the next step, crystalline Tobra powder (donated by a Brazilian company) was solubilized in 200 mL of distilled water in concentrations of 0.0005 g/mL; 0.0015 g/mL; 0.0030 g mL. Then, 30 g of PLA/BCP powders were added to a drug solution and the mixture was put in a furnace at 50 °C for 24 h until the water evaporated. The material was macerated and employed to produce the filaments by hot extrusion in a Wellzoom Desktop filament extruder line II. The extrusion was carried out at a speed of 18 rpm and a temperature of 168 °C in both the preheating zone and extrusion zone. The samples with the different Tobra quantities were obtained and characterized, and the compositions were (in grams): PLA/BCPs/Tobra of 25/5/0.1 (sample F1), 25/5/0.3 (sample F2) and 25/5/0.6 (sample F3).

2.2 Structural and morphologic characterization

The obtained samples i.e., PLA, BCPs, Tobra (crystalline) and Tobra/PLA/BCP (filament with high drug loaded) were analyzed by X-ray powder diffraction (XRPD) analysis, which were performed using a STOE Stadi-P high-resolution diffractometer operating in transmission mode, equipped with a CuKα$_1$ source (λ = 1.54056 Å). The samples were loaded between two cellulose-acetate foils. Data collection was performed in the range from 2 to 40° (2θ). The Rietveld refinement [38] was also performed for the HAP/BCP sample to quantify the phases in the sample. The Topas-Academic V7 software program [39] was used to perform the refinement. The lattice parameters and the crystallite size broadening were refined, and the background was adjusted using a Chebyshev polynomial function with 10 terms.

Fourier transform infrared spectroscopy (FTIR) spectra were recorded on a Shimadzu IRTracer-100 Fourier transform Infrared spectrometer with an accessory for measurements in transmittance (*DRIFTS*). The spectra were acquired in the spectral range between 450 and 4000 cm^{-1} and each spectrum was the average of 3 scans with resolution of 4 cm^{-1}. The thermal properties of the samples were investigated by recording the obtained DSC curves, with a heating rate of 10 °C/min and temperature range from 30 to 300 °C, using a DSC (DSC7020 Exstar, SII NanoTechnology Inc., Tokyo, Japan). The TG/DTG curve was recorded using a horizontal thermobalance 7200 (Exstar, SII NanoTechnology Inc., Tokyo, Japan), heating rate of 10 °C/min, under a 100 ml/min nitrogen flow and temperature range from 30 to 600 °C. Morphology of the printed scaffold was evaluated by Scanning Electron Microscopy (SEM, EVO MA10 Carl Zeiss microscope).

2.3 Drug release assays

High-Performance Liquid Chromatography (HPLC) was used to quantify tobramycin. A Chromaster HPLC device from Hitachi (Japan) equipped with a diode-array detector was used to scan at a wavelength of 245 nm. A Synergi 4 μm Hydro-RP 80 Å column (4.6 × 150 mm) with C-18 cartridges as the precolumn (Phenomenex, USA) were used. The mobile phases were A: 100% Water type I (1% TFA) and B: 100% methanol, at 30 °C temperature. The program was established as follows: initial condition of 40% of B for 1 min, then a linear gradient of 40 to 80% of B in the next 2 min and holding it for 5 min, then returning to the initial condition at 5 min, and equilibrating for 5 min before the next sample injection. A total of 15 μL of the derivatized sample was injected into the HPLC system and separated at 30 °C of temperature, using a constant flow rate of 1 mL/ min.

Next, 500 μL aliquot of each sample was transferred to a 5 mL glass test-tube to perform the derivatization procedure. Then it was mixed again after adding 500 μL of

H_3BO_3–$Na_2B_4O_7$ buffer (pH 9.0), 500 µL of methanol and 200 uL of 4-Chloro-3,5-dinitrobenzotrifluoride (CNBF) methanol solution (8 g/L) to the tube in order. The solution was subsequently incubated at 60 °C for 10 min in a thermostatic water bath. The reaction was quenched by addition of 10 µL of 2 M HCl, and the reaction mixture was diluted to 2 mL with ultrapure water. The resulting solution was filtered through a 0.22 µm nylon filter. After cooling, the derivatized sample was injected into the HPLC system [40].

Finally, drug-release assays were performed at the end of the calibration process. For this purpose, 1 cm long F1, F2 and F3 filaments were used, randomly distributed in 8 individual samples with 1 mL of PBS each. The samples were placed in an incubator at 32 °C with a constant shaker and a sample was taken from each treatment after the times: 0.5, 1, 2, 4, 8, 12, 24, and 48 h. Each sample was derivatized and analyzed using the HPLC system.

2.4 Antimicrobial assay

The inhibition zone of *Staphylococcus aureus* (ATCC ®29,213™) was evaluated to determine the potential antibacterial properties of filament and scaffolds. The bacterial inoculum was initially seeded in Luria–Bertani (LB) broth nutrient, and then subcultured on a petri dish. Previously sterilized filaments (F1, F2, F3) and printed scaffolds with the filaments were then placed in the center of petri dish and maintained at 37 °C for 18 h. The test was carried out in duplicate. After incubation, the presence of bacterial growth inhibition halos (zone of inhibition) around the samples were observed and their diameters in millimeters were measured with a digital caliper (Mitutoyo Corp., Kawasaki, Japan). A Ceftriaxone disk (30 µg/disk) was utilized as positive control.

2.5 Minimum Inhibitory concentration (MIC) determination

The serial dilution method was used to study the antimicrobial efficacy of the Tobra by evaluating the visible growth of S. aureus microorganisms. First, Tobra was diluted in PBS and 1:2. Serial dilutions were made in LB culture medium (Luria Bertani) and added to 96-well plates, Inoculum of the S. aureus ATCC strain was prepared at a concentration of 0.5 on the McFArland scale and was added to each of the wells. Concentrations tested were 400 µg/ml until 0.048 µg/ml. As controls of the test were carried out the sterility of the culture medium and the growth of the bacteria.

3 Results and discussion

The XRPD analysis was performed to characterize the compound samples as well as the high drug loaded sample. Figure 1a shows the Rietveld plot of the HAP/BCP sample that was synthesized by the solution combustion method. The phases identified in this sample were hydroxyapatite (HAP) and β-tricalcium phosphate (β-TCP), and the crystal structures used in the refinement were obtained from the Inorganic Crystal Structure Database®, ref codes #56,306 and #97,500, respectively. The agreement factors obtained from the refinement were $R_{wp} = 4.65\%$ and $\chi^2 = 2.04$, and these indexes together with the well-adjusted Rietveld plot indicate a good result for the refinement. The quantitative phase analysis by the refinement data showed that the BCP sample is composed of 75.2(3)% of HAP and 24.8(3)% of β-TCP (in weight percent). The phases identified in the samples have potential use in bone tissue regeneration because they combine the stability of the apatite phase with the degradability of the tricalcium phosphate [41]. These powders
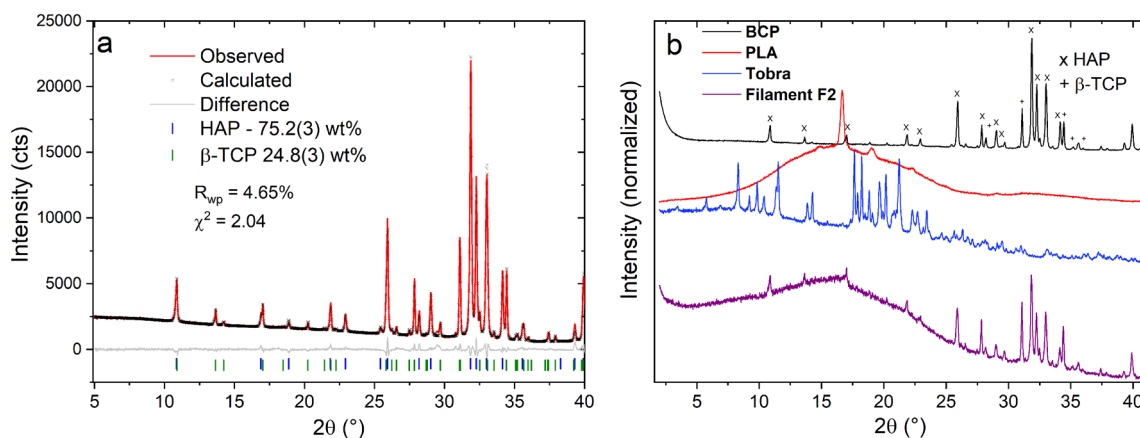
Fig. 1 **a** Rietveld plot of sample BCP, with hydroxyapatite and β-TCP phases; **b** patterns for the isolated components BCP, PLA, Tobra, and the filament with high drug amount samples (the plots were normalized for comparison concerns)

were used to obtain the filaments characterized throughout the manuscript.

The XRPD patterns of the isolated filament components are presented in Fig. 1b (i.e., BCP (black line) with indication of the phases, PLA (red line) and the crystalline Tobra (blue line), as well as the high drug loaded-filament pattern (purple line)). The PLA pattern indicates the semi-crystalline nature for this component, with a characteristic amorphous halo between 15 and 30° and the peaks around 14.80, 16.66° (intense peak), 19.06 and 22.38° (2θ), in good agreement with those peaks reported by Gómez-Pachón et al. [42].

Tobra sample is crystalline with the five characteristic highest intensity diffraction peaks around 8.29, 11.49, 17.67, 18.23 and 21.23° (2θ, using CuKα radiation), in agreement with the pattern reported by Dash (1966) [43] for the anhydrous phase of the sample heated up to 208 °C, indicating that the Tobra analyzed herein is a pure phase sample. This drug has no crystal structure reported yet. Therefore, the indexing procedure was performed considering the first 23 reflections of drug pattern and the crystal structure was indexed on a primitive monoclinic unit cell in a space group $P2_1$, and the lattice parameters obtained from the Pawley refinement [44] were: $a = 25.566(3)$ Å, $b = 19.180(1)$ Å, $c = 5.0908(4)$ Å, $β = 92.224(9)$°, $V = 2494.4(4)$ Å^3. The fitting plot is shown in Figure S1 (supplementary material).

The filament sample with loaded drug does not have any crystalline contribution either from the Tobra crystal structure or from the PLA sample. This can be associated with the fact that during the hot melt extrusion process the temperature corresponding to 168 °C can melt the drug and the PLA component. Therefore, the solidification of the filament after the extrusion process limited the long-period three-dimensional reordering at the atomic level of the PLA as well as the Tobra crystalline structure. The peaks observed for this sample are related to BCP phases, agreeing with the pattern observed for the BCP sample.

An FTIR analysis was performed to evaluate the main functional groups in pure Tobra. This result was used to evaluate the presence of the drug in the filaments, as well as to observe the preservation of the drug molecule after obtaining the filament. The spectrum of pure drugs is shown in Fig. 2a. The bands that were identified at 3452 cm^{-1} correspond to OH stretching, at 3351 cm^{-1} due to N–H stretching, around 2898 cm^{-1} due to C–H stretching, around 1597 cm^{-1} due to N–H bending, at 1470 cm^{-1} due to CH$_2$ scissoring, at 1382–1351 cm^{-1} due to O–H in-plane bending, and at 1034 cm^{-1} due to C–O stretching [15]. Figure 2b shows the FTIR spectrum for PLA and F3. Both spectra resemble each other, except for the highlighted region in which a band appears around 1090 cm^{-1}. A comparison between F2, F3 (high drug amount loaded samples) and the pure drug was performed in Fig. 2c to assure that the contribution observed
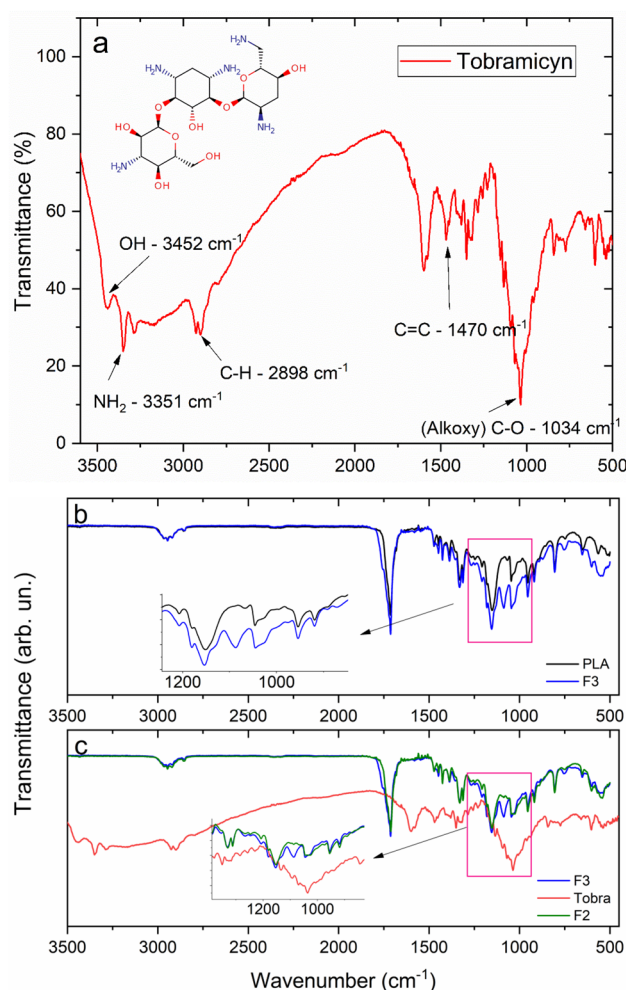
Fig. 2 FTIR spectra of **a** Tobra, **b** PLA and F3, and **c** F3, Tobra and F2 samples

around 1090 cm^{-1} is not related to the BCP phases. It is worth noting that the BCP phases were in the same amount for all samples. In comparing the F3 and F2 spectrum, it is possible to observe that the band around 1090 cm^{-1} is present in the F3 and has a subtle contribution in the F2 sample, indicating that it could be related to the drug C–O functional group. Although Tobra is in small amount in the samples, this band significantly increases when there is double the amount of the drug (i.e., from F2 with composition (g) of 25/5/0.3 (PLA/BCP/Tobra) to F3 with composition (g) of 25/5/0.6 (PLA/BCP/Tobra)). The F1 sample spectrum (not shown) did not present this band, probably due to its low amount in the sample.

The DSC thermograms are presented in Fig. 3. Tobra purity was also probed by DSC indicating that the sample has 99.66% of purity. The DSC curve of Tobra (Fig. 3a) shows a sharp endothermic peak at 138.9 °C, which can be attributed to the melting of the crystalline phase. It is worth noting that one melting peak was observed
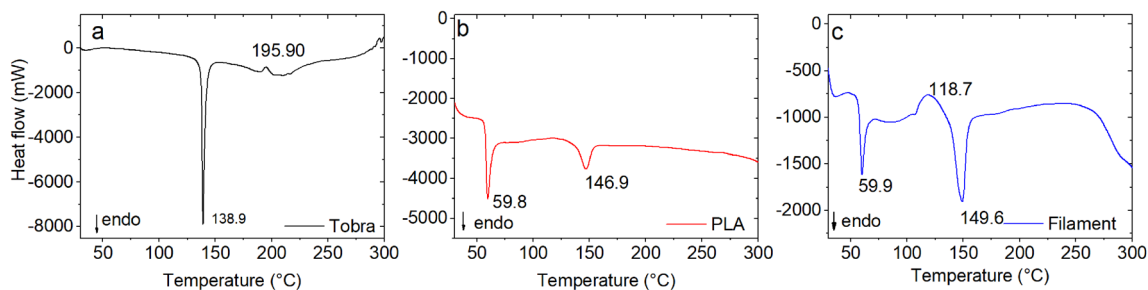
Fig. 3 DSC analysis of Tobra, PLA and filament samples

indicating the presence of only one crystalline phase. Dash and Suryanarayanan [45] characterized tobramycin monohydrate, showing that the dehydration process occurs under increasing temperature and that the observed thermal events were not readily reversed during the cooling of the sample. In our case, we did not observe any thermal event before the melting temperature (T_m), which can be related to a drug anhydrous phase. The T_m observed around 138.9 °C is much lower than reported in the literature (216.78 °C), suggesting that these phases are different. The Tobra XRPD pattern agrees with that obtained for the sample under heat treatment [42], although no thermal analysis was performed for the mentioned heated sample. An exothermic event was also observed around 195.90 °C which can be related to the crystallization event of another polymorph. However, the degradation of the sample occurs before observing a second melting event, as was observed by TG analysis.

Figure 3b shows the DSC of pure PLA with two characteristic peaks associated with glass transition related to the amorphous part of the structure around 59.8 °C and melting point related to the crystalline arrangement around 146.9 °C [46]. The semi-crystallinity of the PLA sample was also observed by XRPD characterization (Fig. 1b, red line).

The filament's thermogram is shown in Fig. 3c, wherein it is possible to observe three events. The first endothermic event is the glass transition around 59.9 °C. The exothermic event around 118.7 °C is due to the crystallization of the PLA structure induced by the temperature increasing during the analysis. This result agrees with what was observed by XRPD analysis for the filament sample, which showed crystalline contribution from HAP and BCP phases and initially amorphous contribution for the PLA compound [46]. The third endothermic event at 149.6 °C can be associated with the melting of the crystalline reordered PLA semi-crystalline structure. The endothermic peak related to Tobra fusion was absent, which indicates a disarrangement of the crystalline structure ordering, indicating that the molecules of this drug can be randomly dispersed in the polymer chains.
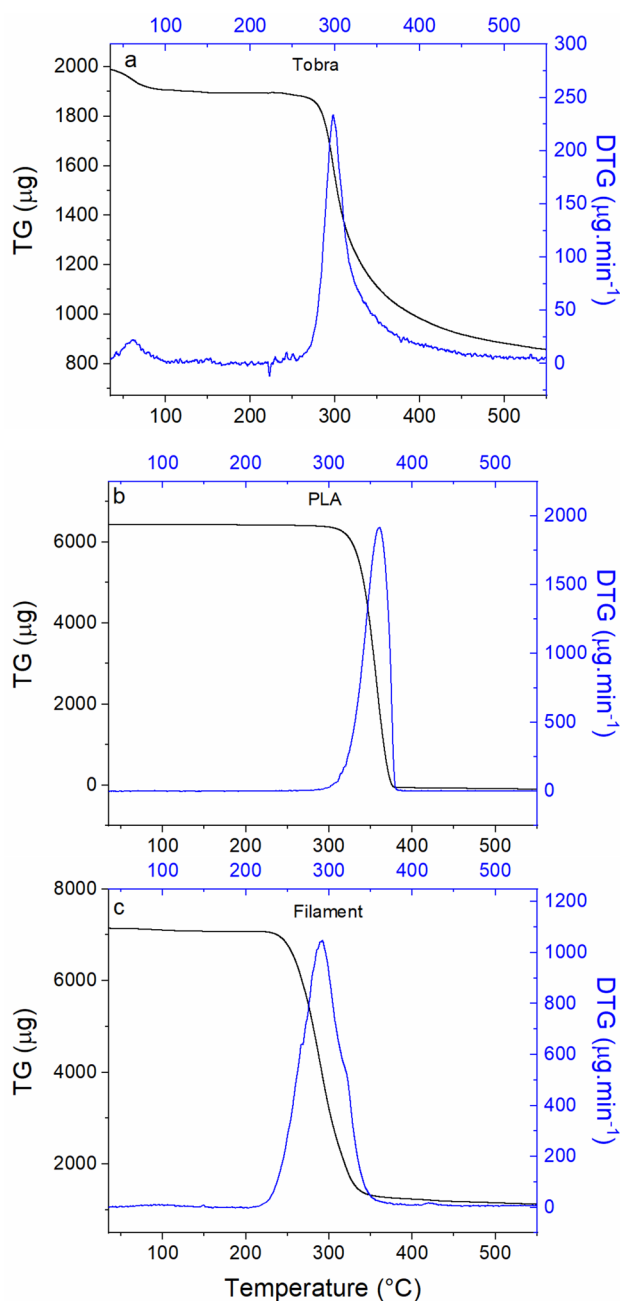
The thermogravimetry (TG) and derivative analysis are presented in Fig. 4. The DTG of the pure Tobra (Fig. 4a) indicates a weight loss up to around 90 °C, which can be

related to adsorbed water in the sample. No other loss was observed until the degradation of the sample, i.e., over 260 °C (maximum around 300 °C), suggesting there was no coordinated water in the sample implying that the Tobra sample was an anhydrous phase. The DTG of PLA revealed only one mass loss with a maximum event at 350 °C. The DTG of the filament sample presents a broad mass loss event between 240 and 350 °C, which can be the superimposed thermal events from the pure compounds.

Figure 5 shows the images of the filament obtained by the hot extrusion procedure, the pieces printed using this manufactured material and the micrograph of the printed scaffold. Figure 5a shows the filament obtained by hot extrusion with an approximate diameter of 1.75 mm suitable for FDM printing, while Fig. 5b shows the SEM image of the filament. It is possible to observe an irregular morphology with the presence of aggregates associated with the calcium phosphates, which is characteristic of the processing where complete homogeneity of the ceramic phase in the polymeric phase is not achieved (5c, d), similar to a previous report [24]. Thus, the printing of cylinder-type controlled geometries was made with this filament in a commercial 3D printer machine (Fig. 5e, f), which shows the printing threads deposited by organized layers typical of the 3D printing process.

The EDS analysis to identify the distribution of phosphates in the printed threads can be viewed in Fig. 5g, and it is possible to identify that with the printing process the phosphates added to the filament are distributed homogeneously on the surface. This behavior in the printing could favor the mineralization processes of new bone and improve the bioactivity of the scaffolds.

Figure 6 shows the chromatograms obtained from different matrices derivatized with CNBF T, and the derivatization method produced 4 peaks in the chromatograms, which corresponds to the derivatization of 4 of the 5 amine groups of tobramycin with retention times of 3.9, 4.7, 5.3 and 5.5 min; in addition, another two signals can also be observed corresponding to hydrolyzed-CNBF (CNBF-OH) and CNBF with retention times of 6 and 7.1 min [39, 47, 48]. Derivatization is widely applied in molecules like tobramycin which do not

Fig. 4 Thermogravimetry and derivative thermogravimetry analysis of **a** Tobra, **b** PLA and **c** filament samples

have absorbance at UV–Visible spectra. Tobramycin has five primary amine groups which can be derivatized, especially the amine group which binds to CH_2, and is the most reactive. CNBF is an excellent derivatization reagent, usually common with many types of molecules such as amino acids [47, 48].

The calibration curve of derivatized tobramycin with retention time of 4.7 min was performed between the range 1.6–200 ug/mL (Fig. 7a).

Each sample taken from the drug-release assay was derivatized and analyzed using the HPLC system. Tobramycin released from the F1 and F2 filament is barely detectable after 4 h (1.5 µg/mL), reaching 4.8 µg/mL in 8 h and a maximum of 7.4 µg/mL for F1 and 10.9 ug/mL for F2 in 48 h of assay. On the other hand, the F3 filament releases 3.4 µg/mL in half an hour, exceeds 10 µg/mL in just one hour and continues to release tobramycin steadily up to 48 h of testing, where 150 µg/mL was detected (Fig. 7b). All samples were compared by unidirectional ANOVA. There are significant statistical differences between the filaments ($P = 0.0144$), and it is evident by observing the multiple comparison that the difference is between the F3 treatment versus the others.

DSC-TG and drug-release analysis suggest an interaction between the drug and the PLA/BCP system. This can be related to the environment generated around the drug due to the mechanism for obtaining the filament, the nature of each of the phases and the physico-chemical properties. Tobra is a hydrophilic aminoglycoside and therefore soluble in aqueous phases, but of limited application in hydrophobic systems such as PLA where polymer-drug interactions are weak.

In our case, the processing technique for obtaining the filament, i.e., an initial dissolution of the drug in an aqueous medium and subsequent mixing with PLA/BCP could favor that Tobra molecules interact through secondary bonds with the BCPs and, in turn, can present some type of weak interaction with the polymer chain. Later, after the evaporation of the solvent the mixture was subjected to hot extrusion processing at a temperature of 168 °C which is above the melting temperature for Tobra and PLA; during this stage both compounds can experience structural changes, such as the amorphization of Tobra and semi-crystallinity for PLA. It is worth noting that the processing temperature is below the drug's degradation temperature observed by the TG analysis (higher than 260 °C).

During the extrusion process the raw materials are subject to mass transport conditions in a viscous fluid, where the majority component (in this case the PLA) acts as the main matrix. Once the temperature of the system is below the glass transition temperature of PLA, the drug can be encapsulated in the PLA/BCPs matrix. This type of interaction is supported by the drug-release mechanism which was found to fit by Korsmayer-Peppas model where it was obtained a high correlation for which the variable $n > 0.5$ indicates that the release of this polymeric system does not only correspond to a Fickian model but also can be associated with the degradation of the matrix, indicating that Tobra is found in a greater amount encapsulated (Table 1). Therefore, the intermolecular interactions between the matrix and the drug's molecules (van der Waals, hydrogen bonds) can promote the stabilization of the amorphous drug, avoiding its recrystallization right after the filaments manufacturing [49]. The drug amorphous state in the filament was observed by the XRPD

Fig. 5 a Image of the filament 1.75 mm; **b–d** SEM image of filament; **e** Printed scaffold; **f** Printed threads with the filament; **g** EDS analysis to identify the distribution of phosphates in the printed threads
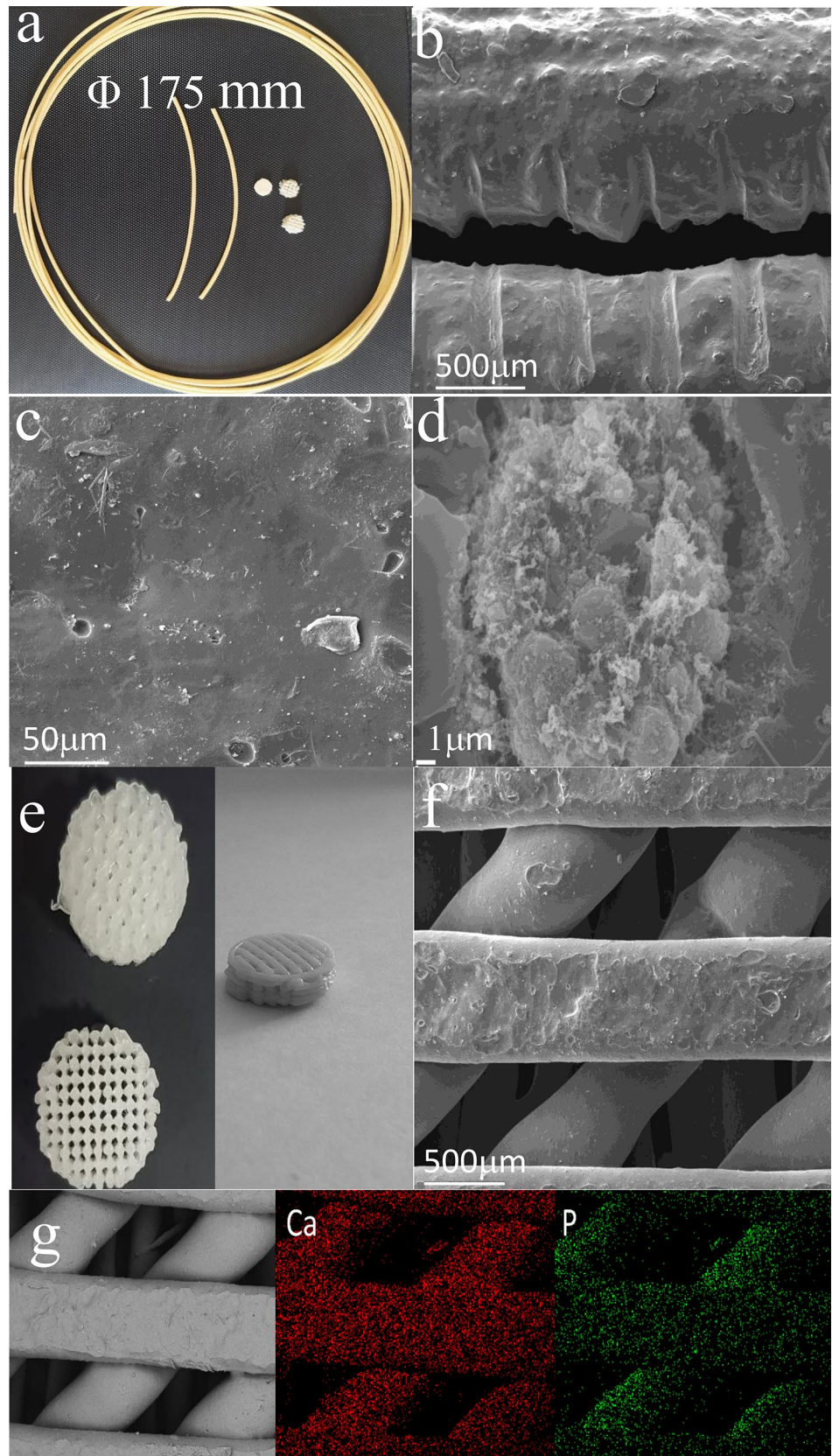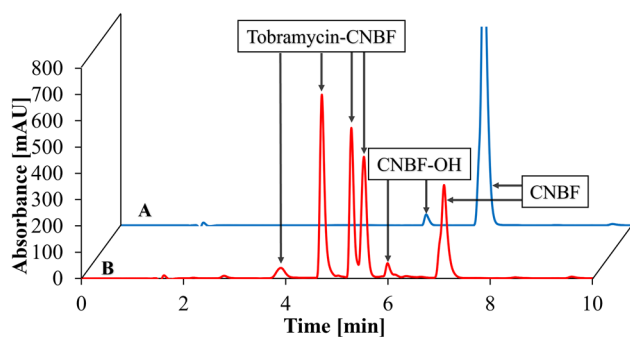
Fig. 6 Chromatograms obtained from different matrices derivatized with CNBF. **A** methanol with CNBF; **B** derivatized Tobramycin

characterization and the drug's molecule preservation was accessed through FTIR analysis, as discussed previously.

The ability of the filaments and the 3D-printed disks to inhibit bacterial growth on *S. aureus* are shown in Figs. 8, 9. It is possible to observe how the control of filament and the piece printed with this filament did not present inhibition halos (Figs. 8, 9a–b) and showed similar behavior to the non-inhibition control, presenting uniform distribution of bacterial colonies within the culture. The presence of an inhibition zone around the filament (Fig. 8c–e) and the printed pieces (Fig. 9d–e) evidence antibacterial activity based on the diffusion of biocidal agent through the culture medium and a clear increase in the inhibition zone as the tobramycin concentration delivery increased. On the order hand, the MIC value calculated for tobramycin was 3.124 µg/mL (supplementary material S3), this inhibition value compared with release profile of filaments shows that the material are supplying the appropriate amounts of Tobra to generate inhibition i.e., the F1 and F2 filaments in the first 8 h present around the 4.8 µg/mL, while the F3 filament from the first hour the concentration of released drug doubles the MIC.

In the case of the printed pieces, it was possible to calculate the size of the inhibition zone with respect to the control (ciprofloxacin sensidisk) and the results are shown in Table 2. These results are also consistent with what was observed in the release of the drug, since the scaffolds that

presented the highest inhibition percentage (up to 67.7%) are those corresponding to those manufactured with the F3 filament, which has a release of up to 150 in 48 h, while the scaffolds manufactured with the F1 and F2 filaments have inhibition percentages of 29.03 and 45.16, respectively. These results validate how even after reprocessing the filament in 3D printing, in which the system is again subjected to a high temperature that in principle could affect the antimicrobial response, the effect does not disappear.

4 Conclusions

Filaments composed of calcium phosphates with antimicrobial response were successfully manufactured by hot extrusion process. These filaments proved to be suitable for use in FDM technologies for scaffold printing. The preservation of the drug in the filament samples was demonstrated by XRPD and FTIR analysis, validating the presence of the drug in the composite filament. It was also observed by XRPD that the crystalline active pharmaceutical ingredient was amorphized after the filament manufacture procedure and was kept in the amorphous state in the filament.

Table 1 Parameters of the mathematical models of adjustment of drug release

| Filament	Model	K	n	$R2$
F1	Zero order	0.134	N.A	0.821
	First order	0.244	N.A	0.607
	Higuchi	0.895	0.500	0.848
	Korsmayer-Peppas	0.610	0.620	0.843
F2	Zero order	0.226	N.A	0.949
	First order	0.067	N.A	0.778
	Higuchi	1.448	0.500	0.968
	Korsmayer-Peppas	0.826	0.674	0.968
F3	Zero order	3.055	N.A	0.943
	First order	0.058	N.A	0.734
	Higuchi	21.958	0.500	0.989
	Korsmayer-Peppas	18.005	0.562	0.986

Fig. 7 **a** Calibration curve of tobramycin-CNBF; **b** Release of tobramycin from the treatments
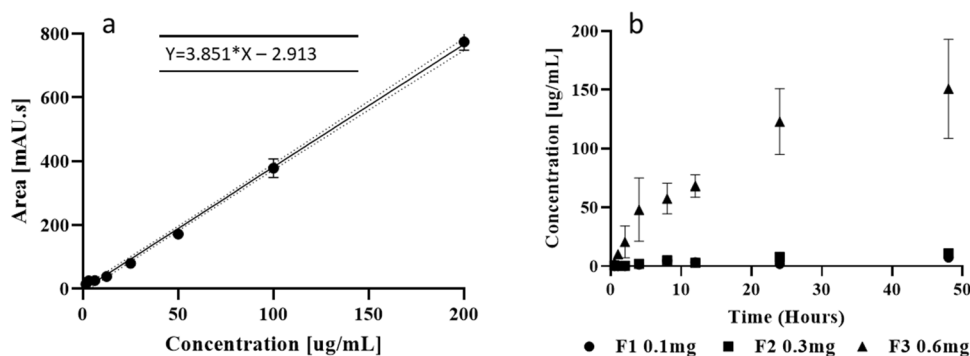
Fig. 8 Antimicrobial assay of filaments. **a**, **b** Filament control without Tobra; **c** F1- filament; **d** F2- filament; **e** F3- filament; **f** ciprofloxacin sensidisk, positive control
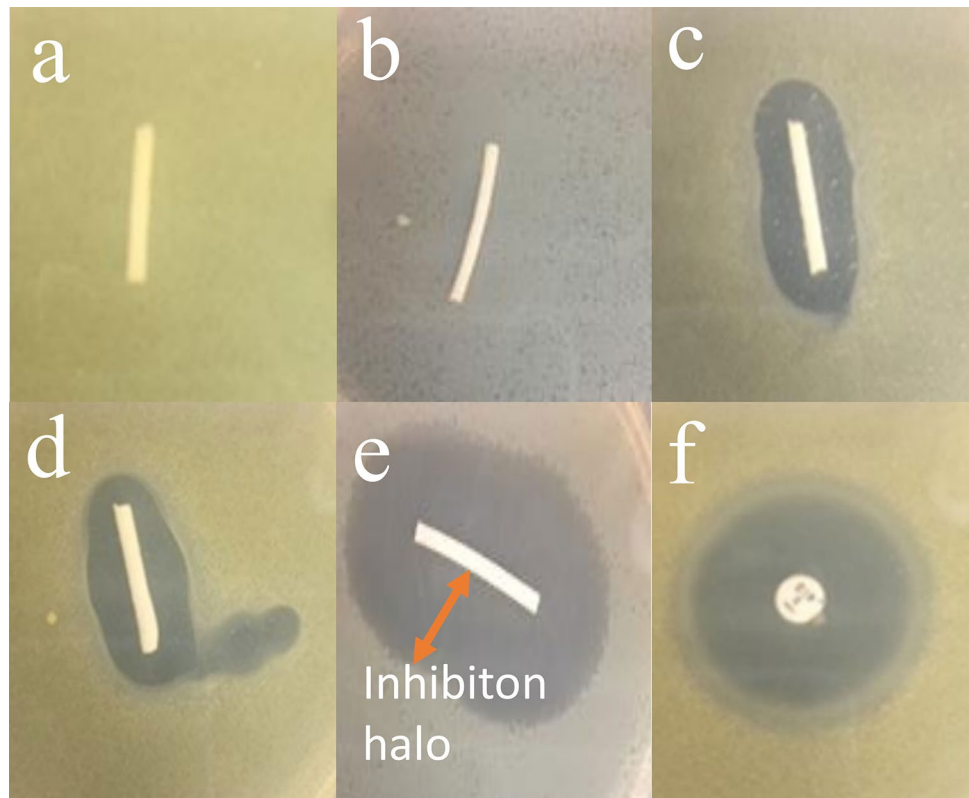
Fig. 9 Antimicrobial assay of 3D-printed scaffolds. **a** Scaffold with filament control without Tobra; **b** Culture control; **c** Ciprofloxacin sensidisk control; **d** Scaffold-Filament F1; **e** Scaffold-Filament F2; **f** Scaffold-Filament F3
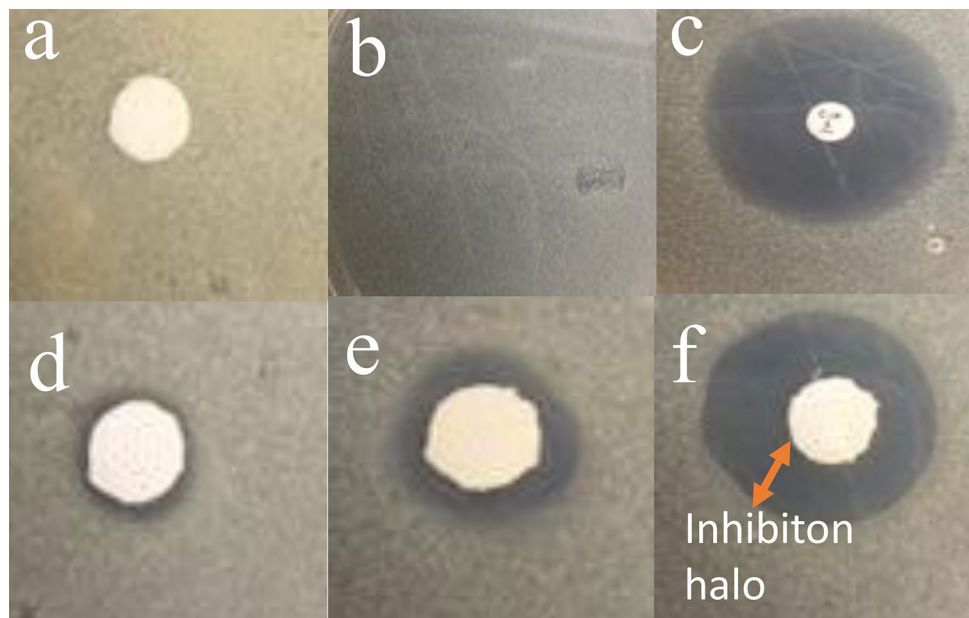
FTIR indicated the presence of C–O functional group that could be related to the drug. The thermal analyzes enabled observing the typical behavior of PLA with a melting temperature around 150 °C and no peaks related to thermal degradation were seen for the temperatures at which the printing of PLA based filaments is usually carried out (150–210 °C).

The release results using the derivation technique showed that the F3 filament with the highest concentration of drug was able to release up to 150 μg in 48 h, which was consistent with the inhibition halos and MIC, with the F3 filament and the scaffolds manufactured with it being those which presented the highest inhibition percentages compared to the

Table 2 Inhibition halos, antimicrobial assay

Sample	Inhibition halos (mm)	
	S. aureus	%
Scaffold-Filament control	0	0
Scaffold-Filament F1	9	29.03
Scaffold-Filament F2	14	45.16
Scaffold-Filament F3	21	67.74
No inhibition control	0	0
Ciprofloxacin sensidisk control	31	100

control. These results validate that it is possible to obtain an antimicrobial filament by hot extrusion with potential application in manufacturing scaffolds by 3D printing without the use of solvents, in turn providing an environment-friendly product and is a great possibility to be used in the biomedical applications in the future.

Declarations

Conflict of interest The authors declare that they have no known competing financial interests or personal relationships that could have appeared to influence the work reported in this paper. The authors declare that they have no conflict of interest.

References

1. C. Wang, W. Huang, Y. Zhou, L. He, Z. He, Z. Chen, X. He, S. Tian, J. Liao, B. Lu, Y. Wei, M. Wang, 3D printing of bone tissue engineering scaffolds. Bioact. Mater. **5**, 82–91 (2020). https://doi.org/10.1016/j.bioactmat.2020.01.004

2. S. Yuan, S. Li, J. Zhu, Y. Tang, Additive manufacturing of polymeric composites from material processing to structural design. Compos. B Eng. **219**, 108903 (2021). https://doi.org/10.1016/J.COMPOSITESB.2021.108903

3. S. Radhakrishnan, S. Nagarajan, H. Belaid, C. Farha, I. Iatsunskyi, E. Coy, L. Soussan, V. Huon, J. Bares, K. Belkacemi, C. Teyssier, S. Balme, P. Miele, D. Cornu, N. Kalkura, V. Cavaillès, M. Bechelany, Fabrication of 3D printed antimicrobial polycaprolactone scaffolds for tissue engineering applications. Mater. Sci. Eng., C **118**, 111525 (2021). https://doi.org/10.1016/j.msec.2020.111525

4. L. Viidik, J. Vesala, R. Laitinen, O. Korhonen, J. Ketolainen, J. Aruväli, K. Kirsimäe, K. Kogermann, J. Heinämäki, I. Laidmäe, T. Ervasti, Preparation and characterization of hot-melt extruded polycaprolactone-based filaments intended for 3D-printing of tablets. Eur. J. Pharm. Sci. **158**, 105619 (2021). https://doi.org/10.1016/J.EJPS.2020.105619

5. S.K. Hedayati, A.H. Behravesh, S. Hasannia, O. Kordi, M. Pourghaumi, A.B. Saed, F. Gashtasbi, Additive manufacture of PCL/nHA scaffolds reinforced with biodegradable continuous Fibers: mechanical properties, in-vitro degradation profile, and cell study. Eur. Polymer J. **162**, 110876 (2022). https://doi.org/10.1016/J.EURPOLYMJ.2021.110876

6. R. Tylingo, P. Kempa, A. Banach-Kopeć, S. Mania, A novel method of creating thermoplastic chitosan blends to produce cell scaffolds by FDM additive manufacturing. Carbohyd. Polym. **280**, 119028 (2022). https://doi.org/10.1016/J.CARBPOL.2021.119028

7. M. Calì, G. Pascoletti, M. Gaeta, G. Milazzo, R. Ambu, New filaments with natural fillers for FDM 3D printing and their applications in biomedical field. Procedia Manuf. **51**, 698–703 (2020). https://doi.org/10.1016/J.PROMFG.2020.10.098

8. M. Olam, N. Tosun, 3D-printed polylactide/hydroxyapatite/titania composite filaments. Mater. Chem. Phys. **276**, 125267 (2022). https://doi.org/10.1016/J.MATCHEMPHYS.2021.125267

9. J.D. Caplin, A.J. García, Implantable antimicrobial biomaterials for local drug delivery in bone infection models. Acta Biomater. **93**, 2–11 (2019). https://doi.org/10.1016/J.ACTBIO.2019.01.015

10. A.F. Widmer, New developments in diagnosis and treatment of infection in orthopedic implants. Clin. Infect. Dis. **33**, S94–S106 (2001). https://doi.org/10.1086/321863

11. R. Teixeira-Santos, M. Lima, L.C. Gomes, F.J. Mergulhão, Antimicrobial coatings based on chitosan to prevent implant-associated infections: A systematic review. IScience. **24**, 103480 (2021). https://doi.org/10.1016/J.ISCI.2021.103480

12. R. Scaffaro, A. Maio, L. Botta, E.F. Gulino, D. Gulli, Tunable release of chlorhexidine from polycaprolactone-based filaments containing graphene nanoplatelets. Eur. Polymer J. **110**, 221–232 (2019). https://doi.org/10.1016/J.EURPOLYMJ.2018.11.031

13. V. Martin, I.A. Ribeiro, M.M. Alves, L. Gonçalves, R.A. Claudio, L. Grenho, M.H. Fernandes, P. Gomes, C.F. Santos, A.F. Bettencourt, Engineering a multifunctional 3D-printed PLA-collagen-minocycline-nanoHydroxyapatite scaffold with combined antimicrobial and osteogenic effects for bone regeneration. Mater. Sci. Eng., C **101**, 15–26 (2019). https://doi.org/10.1016/J.MSEC.2019.03.056

14. J.J. Water, A. Bohr, J. Boetker, J. Aho, N. Sandler, H.M. Nielsen, J. Rantanen, Three-dimensional printing of drug-eluting implants: Preparation of an antimicrobial polylactide feedstock material. J Pharm Sci. **104**, 1099–1107 (2015). https://doi.org/10.1002/JPS.24305

15. M.A. Rosasco, S.L. Bonafede, S.N. Faudone, A.I. Segall, Compatibility study of tobramycin and pharmaceutical excipients using differential scanning calorimetry, FTIR, DRX, and HPLC. J. Therm. Anal. Calorim. **134**, 1929–1941 (2018). https://doi.org/10.1007/S10973-018-7282-Z

16. M. Loose, K.G. Naber, P. Shields, H. Reinhart, F.M.E. Wagenlehner, Urinary concentrations and antimicrobial activity of tobramycin in healthy volunteers receiving a single oral dose of a novel formulation for improved absorption. Int. J. Antimicrob. Agents **51**, 422–426 (2018). https://doi.org/10.1016/J.IJANTIMICAG.2017.11.004

17. S. Khan, S. Warade, D.J. Singhavi, Improvement in ocular bioavailability and prolonged delivery of tobramycin sulfate following topical ophthalmic administration of drug-loaded mucoadhesive microparticles incorporated in thermosensitive in situ gel. J. Ocul. Pharmacol. Ther. **34**, 287–297 (2018). https://doi.org/10.1089/JOP.2017.0079

18. D.K. Mills, U. Jammalamadaka, K. Tappa, J. Weisman, Studies on the cytocompatibility, mechanical and antimicrobial

properties of 3D printed poly(methyl methacrylate) beads. Bioact. Mater. **3**, 157–166 (2018). https://doi.org/10.1016/J.BIOACTMAT.2018.01.006

19. G.A. Lulu, A. Karunanidhi, L. Mohamad Yusof, Y. Abba, F. Mohd Fauzi, F. Othman, In vivo efficacy of tobramycin-loaded synthetic calcium phosphate beads in a rabbit model of staphylococcal osteomyelitis. Ann. Clin. Microbiol. Antimicrob. **17**, 1–11 (2018)

20. J.Y. Ferguson, M. Dudareva, N.D. Riley, D. Stubbs, B.L. Atkins, M.A. McNally, The use of a biodegradable antibiotic-loaded calcium sulphate carrier containing tobramycin for the treatment of chronic osteomyelitis: a series of 195 cases. Bone Joint J. **96**, 829–836 (2014)

21. M. Hill, R.N. Cunningham, R.M. Hathout, C. Johnston, J.G. Hardy, M.E. Migaud, Formulation of antimicrobial tobramycin loaded PLGA nanoparticles via complexation with AOT. J Funct Biomater. **10**, 26 (2019)

22. F.H. Allen, The cambridge structural database: A quarter of a million crystal structures and rising. Urn: Issn **58**, 380–388 (2002). https://doi.org/10.1107/S0108768102003890

23. S.K. Lan Levengood, S.J. Polak, M.B. Wheeler, A.J. Maki, S.G. Clark, R.D. Jamison, A.J. Wagoner Johnson, Multiscale osteointegration as a new paradigm for the design of calcium phosphate scaffolds for bone regeneration. Biomaterials **31**, 3552–3563 (2010). https://doi.org/10.1016/J.BIOMATERIALS.2010.01.052

24. B. Mohapatra, T.R. Rautray, Strontium-substituted biphasic calcium phosphate scaffold for orthopedic applications. J. Korean Ceram. Soc. **57**, 392–400 (2020). https://doi.org/10.1007/S43207-020-00028-X

25. M. Castilho, C. Moseke, A. Ewald, U. Gbureck, J. Groll, I. Pires, J. Teßmar, E. Vorndran, Direct 3D powder printing of biphasic calcium phosphate scaffolds for substitution of complex bone defects. Biofabrication **6**, 015006 (2014). https://doi.org/10.1088/1758-5082/6/1/015006

26. P. Nevado, A. Lopera, V. Bezzon, M.R. Fulla, J. Palacio, M.A. Zaghete, G. Biasotto, A. Montoya, J. Rivera, S.M. Robledo, H. Estupiñan, C. Paucar, C. Garcia, Preparation and in vitro evaluation of PLA/biphasic calcium phosphate filaments used for fused deposition modelling of scaffolds. Mater. Sci. Eng., C **114**, 111013 (2020). https://doi.org/10.1016/J.MSEC.2020.111013

27. C. Yang, O. Unursaikhan, J. Lee, U. Jung, C. Kim, S. Choi, Osteoconductivity and biodegradation of synthetic bone substitutes with different tricalcium phosphate contents in rabbits. J. Biomed. Mater. Res. Part B: Appl. Biomater. **102**, 80–88 (2014)

28. E.-U. Lee, D.-J. Kim, H.-C. Lim, J.-S. Lee, U.-W. Jung, S.-H. Choi, Comparative evaluation of biphasic calcium phosphate and biphasic calcium phosphate collagen composite on osteoconductive potency in rabbit calvarial defect. Biomater. Res. **19**, 1–7 (2015)

29. H.-C. Lim, M.-L. Zhang, J.-S. Lee, U.-W. Jung, S.-H. Choi, Effect of different hydroxyapatite: β-tricalcium phosphate ratios on the osteoconductivity of biphasic calcium phosphate in the rabbit sinus model. Int. J. Oral. Maxillofac. Implants. **30**, 65–72 (2015)

30. A. Piattelli, A. Scarano, C. Mangano, Clinical and histologic aspects of biphasic calcium phosphate ceramic (BCP) used in connection with implant placement. Biomaterials **17**, 1767–1770 (1996)

31. J.-M. Bouler, P. Pilet, O. Gauthier, E. Verron, Biphasic calcium phosphate ceramics for bone reconstruction: A review of biological response. Acta Biomater. **53**, 1–12 (2017)

32. S.E. Kim, K. Park, Recent advances of biphasic calcium phosphate bioceramics for bone tissue regeneration. Biomimicked.

Biomater. (2020). https://doi.org/10.1007/978-981-15-3262-7_12

33. F. Oberdiek, C.I. Vargas, P. Rider, M. Batinic, O. Görke, M. Radenković, S. Najman, J.M. Baena, O. Jung, M. Barbeck, Ex vivo and in vivo analyses of novel 3d-printed bone substitute scaffolds incorporating biphasic calcium phosphate granules for bone regeneration. Int. J. Mol. Sci. **22**, 3588 (2021)

34. Y.W. Seo, J.Y. Park, D.N. Lee, X. Jin, J.K. Cha, J.W. Paik, S.H. Choi, 3-D Printed BCP blocks with different pore sizes for regeneration in rabbit calvarial defects. Res. Sq. (2022). https://doi.org/10.21203/rs.3.rs-1437572/v1

35. V. Wall, T.-H. Nguyen, N. Nguyen, P.A. Tran, Controlling antibiotic release from polymethylmethacrylate bone cement. Biomedicines. **9**, 26 (2021)

36. K.C. Patil, *Chemistry of nanocrystalline oxide materials: combustion synthesis, properties and applications* (World Scientific, 2008)

37. C. Esposito Corcione, F. Scalera, F. Gervaso, F. Montagna, A. Sannino, A. Maffezzoli, One-step solvent-free process for the fabrication of high loaded PLA/HA composite filament for 3D printing. J. Therm. Anal. Calorim. **134**, 575–582 (2018). https://doi.org/10.1007/s10973-018-7155-5

38. H.M. Rietveld, A profile refinement method for nuclear and magnetic structures. Urn: Issn **2**, 65–71 (1969). https://doi.org/10.1107/S0021889869006558

39. A.A. Coelho, TOPAS and TOPAS-Academic: An optimization program integrating computer algebra and crystallographic objects written in C++. Urn: Issn **51**, 210–218 (2018). https://doi.org/10.1107/S1600576718000183

40. S. He, Q. Chen, Y. Sun, Y. Zhu, L. Luo, J. Li, Y. Cao, Determination of tobramycin in soil by HPLC with ultrasonic-assisted extraction and solid-phase extraction. J. Chromatogr. B **879**, 901–907 (2011). https://doi.org/10.1016/J.JCHROMB.2011.02.042

41. R.D. Ventura, A.R. Padalhin, B. Kim, M.K. Park, B.T. Lee, Evaluation of bone regeneration potential of injectable extracellular matrix (ECM) from porcine dermis loaded with biphasic calcium phosphate (BCP) powder. Mater. Sci. Eng., C **110**, 110663 (2020). https://doi.org/10.1016/J.MSEC.2020.110663

42. E.Y. Gómez-Pachón, R. Vera-Graziano, R.M. Campos, Structure of poly(lactic-acid) PLA nanofibers scaffolds prepared by electrospinning IOP conference series. Mater. Sci. Eng. **59**, 012003 (2014). https://doi.org/10.1088/1757-899X/59/1/012003

43. A.K. Dash, Tobramycin. Anal. Profiles. Drug Subst. Excip. **24**, 579–613 (1996). https://doi.org/10.1016/S0099-5428(08)60703-0

44. G.S. Pawley, Unit-cell refinement from powder diffraction scans. Urn: Issn **14**, 357–361 (1981). https://doi.org/10.1107/S0021889881009618

45. A.K. Dash, R. Suryanarayanan, Solid-state properties of tobramycin. Pharm. Res. **8**, 1159–1165 (1991). https://doi.org/10.1023/A:1015858503031

46. P. Maróti, B. Kocsis, A. Ferencz, M. Nyitrai, D. Lőrinczy, Differential thermal analysis of the antibacterial effect of PLA-based materials planned for 3D printing. J. Therm. Anal. Calorim. **139**, 367–374 (2020). https://doi.org/10.1007/S10973-019-08377-4/FIGURES/5

47. T. Tang, T. Shi, K. Qian, P. Li, J. Li, Y. Cao, Determination of biogenic amines in beer with pre-column derivatization by high performance liquid chromatography. J. Chromatogr. B **877**, 507–512 (2009). https://doi.org/10.1016/J.JCHROMB.2008.12.064

48. T. Shi, T. Tang, K. Qian, F. Wang, J. Li, Y. Cao, High-performance liquid chromatographic method for determination of amino acids by precolumn derivatization with

4-chloro-3,5-dinitrobenzotrifluoride. Anal. Chim. Acta **654**, 154–161 (2009). https://doi.org/10.1016/J.ACA.2009.09.027

49. J.M.C. de Assis, E.J. Barbosa, V.D.N. Bezzon, F.R. Lourenço, F.M.S. Carvalho, J.R. Matos, N. Araci Bou-Chacra, C.J. Benmore, S.R. Byrn, F.N. Costa, G.L.B. de Araujo, Hot-melt extrudability of amorphous solid dispersions of flubendazole-copovidone: An exploratory study of the effect of drug loading and the balance of adjuvants on extrudability and dissolution. Int. J. Pharm. **614**, 121456 (2022). https://doi.org/10.1016/J.IJPHARM.2022.121456